

Microscale Combinatorial Libraries for the Discovery of High-Entropy Materials

Lars Banko, Emmanuel Batsa Tetteh, Aleksander Kostka, Tobias Horst Piotrowiak, Olga Anna Krysiak, Ulrich Hagemann, Corina Andronesu, Wolfgang Schuhmann,* and Alfred Ludwig*

Polyelemental material systems, specifically high-entropy alloys, promise unprecedented properties. Due to almost unlimited combinatorial possibilities, their exploration and exploitation is hard. This challenge is addressed by co-sputtering combined with shadow masking to produce a multitude of microscale combinatorial libraries in one deposition process. These thin-film composition spreads on the microscale cover unprecedented compositional ranges of high-entropy alloy systems and enable high-throughput characterization of thousands of compositions for electrocatalytic energy conversion reactions using nanoscale scanning electrochemical cell microscopy. The exemplary exploration of the composition space of two high-entropy alloy systems provides electrocatalytic activity maps for hydrogen evolution and oxygen evolution as well as oxygen reduction reactions. Activity optima in the system Ru–Rh–Pd–Ir–Pt are identified, and active noble-metal lean compositions in the system Co–Ni–Mo–Pd–Pt are discovered. This illustrates that the proposed microlibraries are a holistic discovery platform to master the multidimensionality challenge of polyelemental systems.

applications, their design frequently requires the use of many (3–12) elements in specific combinations and tailored compositional ratios to define their intrinsic properties. In the past, the invention and development of multinary engineering materials such as steels, superalloys, or metallic glasses has taken decades, as an overwhelming number of individual experiments had to be performed to finally understand the influence of alloying and processing on structural and mechanical properties of these materials.^[1] However, today the time for the development of new materials, e.g., electrocatalysts to mitigate climate change, is limited. Disruptive concepts^[2–5] are necessary to accelerate the discovery and the development process of new materials, such as active electrocatalysts for hydrogen evolution, oxygen reduction, and oxygen evolution, which are consid-

1. Introduction

New materials are essential to progress in many areas of modern technology. To meet the manifold requirements of

ered the only hope for a successful implementation of a sustainable hydrogen economy.

Recently, high-entropy alloys (HEAs) have shown their potential to offer paradigm-changing materials design concepts


L. Banko, T. H. Piotrowiak, A. Ludwig
Materials Discovery and Interfaces
Institute for Materials
Faculty of Mechanical Engineering
Ruhr University Bochum
Universitätsstraße 150, D-44801 Bochum, Germany
E-mail: alfred.ludwig@rub.de

E. B. Tetteh, O. A. Krysiak, W. Schuhmann
Analytical Chemistry—Center for Electrochemical Sciences (CES)
Faculty of Chemistry and Biochemistry
Ruhr University Bochum
Universitätsstraße 150, D-44801 Bochum, Germany
E-mail: wolfgang.schuhmann@rub.de

A. Kostka, A. Ludwig
Zentrum für Grenzflächendominierte Höchstleistungswerkstoffe (ZGH)
Ruhr University Bochum
Universitätsstraße 150, D-44801 Bochum, Germany

U. Hagemann
Interdisciplinary Center for Analytics on the Nanoscale (ICAN)
University Duisburg-Essen
Carl-Benz-Straße 199, D-47057 Duisburg, Germany

C. Andronesu
Chemical Technology III
Faculty of Chemistry and CENIDE Center for Nanointegration
University Duisburg-Essen
Carl-Benz Straße 199, D-47057 Duisburg, Germany

 The ORCID identification number(s) for the author(s) of this article can be found under <https://doi.org/10.1002/adma.202207635>.

© 2023 The Authors. Advanced Materials published by Wiley-VCH GmbH. This is an open access article under the terms of the Creative Commons Attribution-NonCommercial-NoDerivs License, which permits use and distribution in any medium, provided the original work is properly cited, the use is non-commercial and no modifications or adaptations are made.

DOI: 10.1002/adma.202207635

for achieving outstanding properties, e.g., as novel electrocatalysts for efficient energy conversion.^[6] Considering the millions of possible combinations of specific elements and their mixing ratios, HEAs open up an enormous composition space with great opportunities for the discovery of new materials. Because of this “combinatorial explosion,” comprehensive sampling of all possible chemical compositions in polyelemental systems is a grand challenge that limits their experimental exploration, i.e., choosing combinations of 5 out of 50 elements results in more than 2×10^6 possible combinations. Experimental exploration by variation of the mixing ratios of constituent elements of each of these element combinations requires, depending on the resolution, fabrication of roughly 10^4 (5 at% steps) or 5×10^6 (1 at%) samples. Additionally, statistical validation and the investigation of optimal processing routes or destructive analysis require repeated synthesis of all these materials. Hence, an ultrahigh number of samples are necessary for the complete experimental investigation of polyelemental systems. This challenge can be addressed by computational modeling,^[7–10] data-driven design,^[11,12] and autonomous materials discovery approaches.^[13] Yet, prior information on the expected variance of the target properties with chemical composition is often missing, and extensive experimentation is indispensable to validate theoretical models and to acquire reliable data for data-driven methods.

Materials discovery and optimization were accelerated by combinatorial materials science,^[14] i.e., fabrication of materials libraries^[15] combined with high-throughput procedures both in experiments^[16] and computation.^[17] Materials libraries, fabricated in “parallel” by co-deposition (e.g., by magnetron sputtering)^[18] or “sequentially” by chemical solution synthesis (e.g., inkjet printing),^[19] comprise hundreds to thousands of chemical compositions. Co-sputtering has the advantage of atomic-scale mixing during deposition and parallel synthesis of high-purity thin films in a single process. Sputtering of HEAs without intentional substrate heating results in fine-grained, nanostructured thin films with grain sizes comparable to particle synthesis techniques, such as carbothermal shock.^[4] Also HEAs comprising elements, which are not mixable in equilibrium, can be obtained.

All combinations of up to ternary systems can be fabricated as continuous composition spreads (i.e., there is no compositional gap as compared to discrete materials libraries) in a single experiment. Advancing to quaternary and higher systems, the number of covered compositions in a materials library is reduced substantially. Compared to ternary systems, where the relative arrangement of deposition sources does not affect the covered composition space (each deposition source is neighbor to all other deposition sources), combinatorial co-deposition of four or more elements produces different composition gradients, depending on the relative arrangement of deposition sources (see Figure S1, Supporting Information). Recently, we reported a strategy to effectively extend the covered compositions of quinary systems by sequential fabrication of materials libraries by permutating the arrangement of individual deposition source.^[20] However, the composition space coverage obtained by this approach still requires a large experimental effort, and covering the total composition space of multinary systems is not feasible. Relating the experimental effort

for covering substantial parts of multinary composition spaces to the number of possible material systems (e.g., quinary combinations) makes it indispensably necessary to develop a disruptive approach for materials discovery.

We overcome the hitherto existing limits of combinatorial materials synthesis by applying a novel, miniaturized shadow masking concept during co-sputtering.^[21] Shadow masking in combination with the tilted flux of species during co-sputtering allows us to generate thin films with arbitrary but well-defined composition gradients over a substrate, i.e., to synthesize compositions, which are typically unavailable in a normal co-deposition setup. Adapting this concept to the microscale is the basis for new high-throughput, micro/nanoscale microscopy characterization possibilities to efficiently screen properties of interest in the microlibraries. We demonstrate this on the example of structural and electrocatalytic properties in a quinary high-entropy alloy. The lift-off lithography mask design enables the synthesis of complete multinary material systems in a single static deposition process. The resulting set of thin-film microlibraries, all containing microscale continuous composition gradients, enables structural characterization using transmission electron microscopy (TEM) and electrocatalytic characterization by means of scanning electrochemical cell microscopy (SECCM).^[22] Three important electrocatalytic reactions, namely the hydrogen evolution reaction (HER), the oxygen reduction reaction (ORR), and the oxygen evolution reaction (OER), are evaluated on quinary composition spreads of Ru–Rh–Pd–Ir–Pt and Co–Ni–Mo–Pd–Pt.

2. Results and Discussion

In a single experiment, the synthesis of a set of microlibraries is achieved by combinatorial co-sputtering from five sources through sets of microscale apertures (Figure 1a) fabricated by lift-off photolithography. The material flux from individual deposition sources, deposited through the microscale circular apertures, produces Gaussian-like deposition profiles on the substrate (Figure 1b), resulting from the angular distribution of deposition fluxes in magnetron sputtering, the deposition source tilt, and the shadowing effects from the aperture mask (see Figure S2, Supporting Information). By appropriate design of the deposition parameters, aperture size, deposition source angle, and distance between mask and substrate, the simultaneous material fluxes from the deposition sources can be separated, and the resulting composition gradients can be controlled by these parameters. Surface composition measurements using Auger electron spectroscopy verify the separation of the elemental deposition profiles (Figure 1c). The composition gradients can be controlled by changing the relative position of the multiple apertures of the mask (Figure 1d). Multiaperture masks are used to create chemical compositions, which are not achievable by a single aperture, e.g., using a pentagon-shaped aperture pattern the deposited composition spreads are extended (see Figure S3, Supporting Information). Numerical simulations supplement the mask design to predefine the fabricated compositions and the composition space coverage (see Figure S4, Supporting Information). The results show that arranging apertures in a ring shape (Figure 1d) and

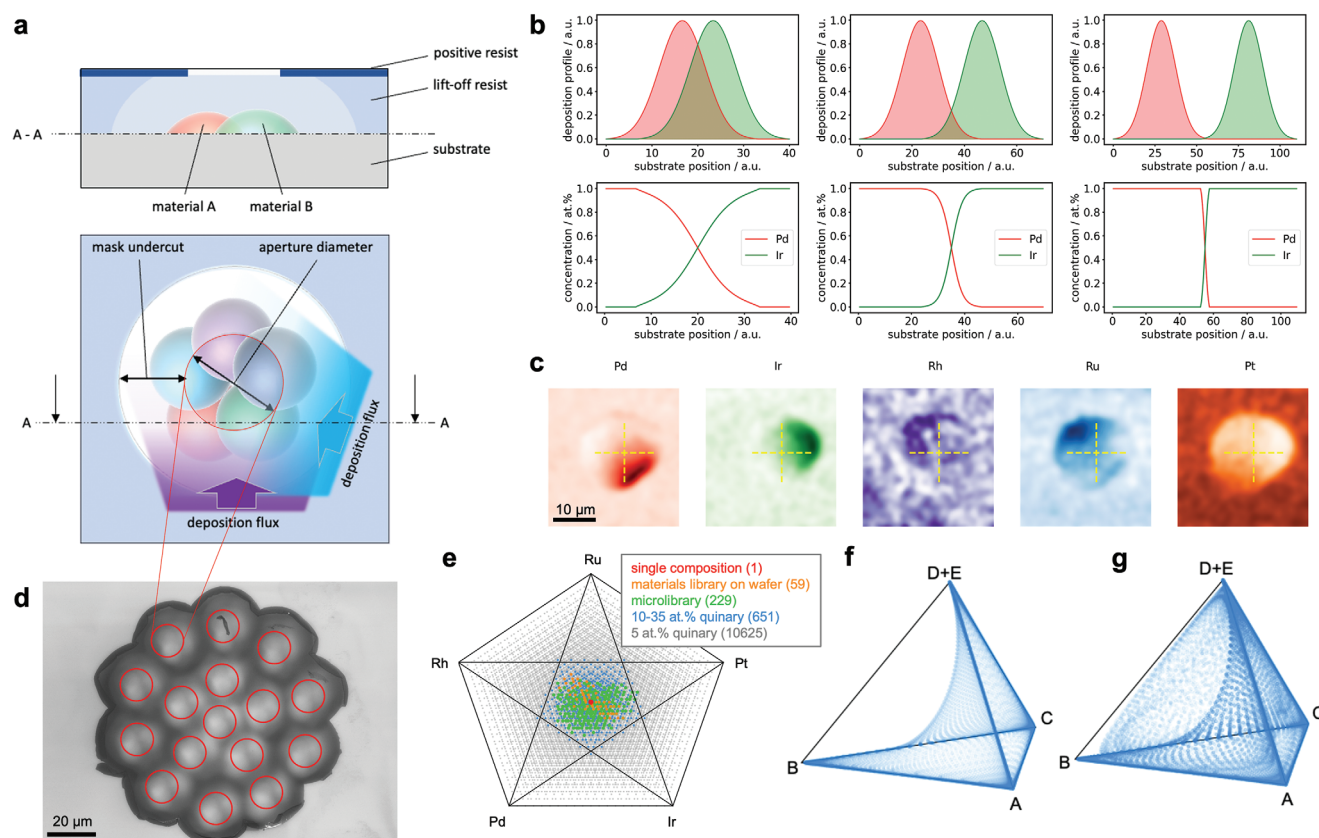


Figure 1. Concept of microlibraries for the holistic synthesis of polyelemental systems. a) As part of a microlibrary, an individual composition gradient is synthesized by co-deposition from five tilted sources through a microscale photolithographic aperture mask (transparent light blue area: undercut area of photoresist). b) Example of calculated Gaussian deposition profiles and resulting composition gradients. c) Color-coded surface element distributions measured by Auger electron spectroscopy on an individual composition gradient (sputtered through a single 5 μm diameter aperture). d) Light microscopy image of a microlibrary; apertures are indicated by red circles. e) Visualization of quinary composition space coverage by a single sample (red), a co-deposited macroscopic materials library (orange), and a microlibrary (green). The number of unique compositions that are covered is indicated. Gray points show all compositions in a quinary system in 5 at% steps, whereas blue points show all possible compositions in a quinary system between 10 and 35 at% in 5 at% steps. f, g) Compositions covered in simulated microlibrary sets: f) a parameter set (mask layout) that only partially covers the composition space while in (g), an optimized aperture mask layout greatly extends the covered compositions.

optimizing the relative distance of apertures maximize the composition space coverage.

The ring-shaped mask design shown in Figure 1d is chosen to cover a composition space centered around equiatomic compositions with a variation of each element between 10 and 35 at%. Figure 1e illustrates the effect of microlibraries in terms of composition space coverage by relating the resulting compositions of different sample fabrication techniques to unique compositions in the quinary composition space. While single sample synthesis produces a single composition, a wafer-scale materials library produces a set of compositions that cover 59 composition steps (out of 10 626 possible compositions). In comparison, a single, exemplary microlibrary produces 229 compositions in a single deposition process. To reach a similar composition space coverage would require synthesis of multiple wafer-scale materials libraries for different deposition source arrangements, which adds an experimental overhead of roughly 10 working days. Simulations indicate that, by further optimization of the aperture mask pattern, nearly complete compositional coverage can be achieved (see Figure 1f, g). By this, all compositions of multinary material systems

(e.g., quinary), included all subsystems (quaternary, ternary, binary, and single elements), could be produced in a single, parallel synthesis process. The small dimensions of a microlibrary (100 \times 100 μm^2) enable the parallel synthesis of thousands of microlibraries (see Figure S5, Supporting Information) which are replications or variations on a typical wafer substrate of 100 mm diameter. Replications can be used for variation of postprocessing of the same composition spread or for different destructive measurements.

A single microlibrary containing multiple continuous gradients can be rapidly explored by scanning microscopy and imaging tools. As an example, the spatially resolved chemical composition of a microlibrary was determined by energy-dispersive X-ray spectroscopy (EDX) using scanning electron microscopy (SEM), and in cross section using TEM. A focused ion beam (FIB) system was used to prepare a cross-sectional sample (Figure 2a) in a region of the microlibrary, which comprises quasibinary composition gradients of Pt and Pd. TEM-EDX was performed along a cross section of the microlibrary (Figure 2b) generating a composition–structure map by acquiring diffraction data at 20 positions along the composition

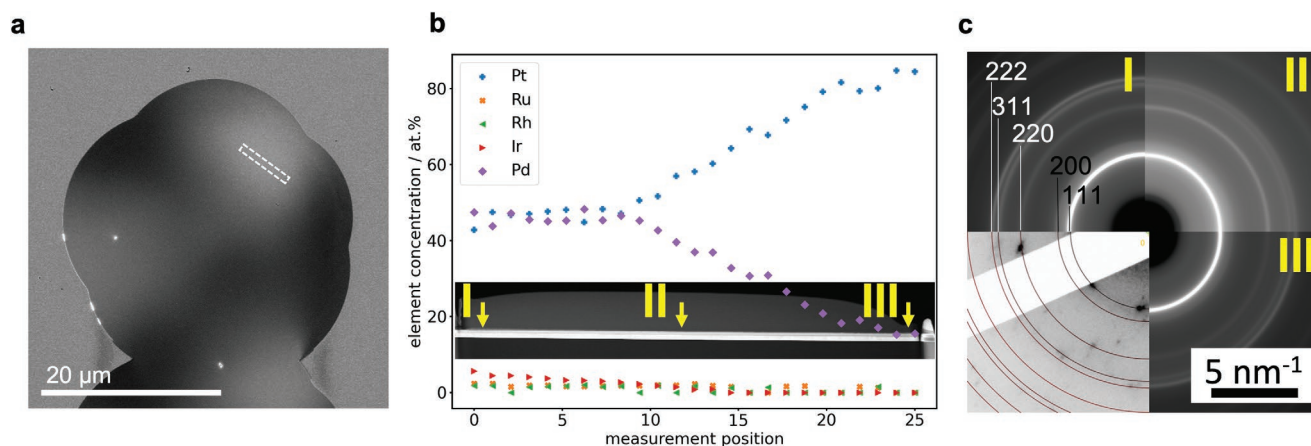


Figure 2. High-throughput nanoscale characterization of microlibraries. a) SEM image of a microlibrary. The position of the FIB-cut cross-sectional sample is indicated. b) Chemical composition along the FIB-cut sample from TEM–EDX. The positions where the diffraction patterns were acquired are highlighted on the high angle annular dark field TEM cross-sectional image (inset). c) Averaged diffraction patterns from the regions highlighted in panel (b) as well as an exemplary raw diffraction pattern with overlaid Pt lines.

gradient (Figure 2c). The results show that microlibraries additionally enable high-throughput experimentation in the TEM, offering a number of well-defined and well-comparable samples.

The microlibrary concept was further used as a basis to study the effect of chemical composition on electrocatalytic properties in the system Ru–Rh–Pd–Ir–Pt. Linear sweep voltammograms (LSV) were acquired using SECCM (tip diameter = 100 nm) on an orthogonal 51×51 grid (hopping distance = 2 μm), covering an area of $100 \mu\text{m} \times 100 \mu\text{m}$. Activity maps that identify areas with higher or lower electrocatalytic activity are generated by comparing the recorded LSVs at defined potentials (Figure 1a), which were –0.1, 0.2, and 1.47 V versus reversible hydrogen electrode (RHE) for HER, ORR, and OER, respectively. By merging chemical composition (Figure 3b) and electrochemical screening data (Figure 3a), one can rapidly identify compositions with promising electrocatalytic properties. The LSV of selected regions of interest are plotted in Figure 3c for detailed comparison. In this exemplary noble-metal HEA system, all compositions show exceptional catalytic performance. However, these results also show that tuning of the chemical composition can be used to optimize the catalytic activity for individual reactions. To demonstrate the versatility of the approach, the system Co–Ni–Mo–Pd–Pt was studied. The results illustrate that the microlibrary approach is effective for identifying promising, especially noble-metal lean catalysts (see Figure S6, Supporting Information).

The complete synthesis–characterization procedure, can be successfully performed in one working day and enables the generation of a dataset that provides composition–electrochemical activity correlation for substantial parts of the high-entropy material composition space (equiatomic center ± 10 at%).

3. Conclusion

Microlibraries fabricated in a single experiment cover substantial parts of high-dimensional composition spaces and thereby enable high-throughput characterization by scanning micro-

scopy methods. We survey electrochemical activities for two high-entropy alloy systems, the exemplary noble-metal system Ru–Rh–Pd–Ir–Pt and the noble-metal lean system Co–Ni–Mo–Pd–Pt. Each system is studied for three electrochemical reactions, yielding datasets of 7800 voltammograms, in less than a working day. The data from this approach cover substantial parts of all possible quinary compositions of high-entropy alloy systems. By optimization of procedures, even higher numbers of compositions could be covered, making it a suitable approach for generating “big data,” which are typically considered nearly impossible in material science. The demonstrated, fast screening concept will substantially accelerate the discovery of urgently needed materials (abundant, non-noble-metal catalysts) for the green energy transition, but is generally applicable to all material classes.

4. Experimental Section

Photolithographic Mask Fabrication: A 100 mm Si wafer with a 500 nm SiO_2 barrier coating was covered with a 50 nm Pt layer to provide an electrically conductive layer for SECCM measurements. Lift-off resist (LOR20B) was spin-coated on the Pt-coated wafer with parameters that resulted in a 4 μm thick coating. The resist was heated at 160 $^\circ\text{C}$ for 60 s and afterward, a positive resist (AZ1518) was spin-coated onto the wafer. The wafer with both resists was heated a second time to 100 $^\circ\text{C}$ for 60 s. The microlibrary aperture mask layout was exposed in a laser lithography system (Heidelberg Instruments). After exposure, the photoresist was developed, resulting in the removal of the exposed areas. Further, an undercut in the lift-off resist was produced during the development.

Synthesis of Microlibraries: Sputter synthesis of the microlibraries was carried out in a co-deposition chamber (DCA) equipped with five magnetrons that were confocally aligned to the substrate at an angle of 45° . The five magnetrons were equipped with pure elemental targets (Ru, Rh, Pd, Ir, and Pt, 99.99% purity). The power for each magnetron was controlled by individual power supplies, such that the chemical composition in the centre of the substrate was approximately equiatomic (20 at% for each element). The deposition was conducted in Ar. The pressure was regulated downstream to 0.5 Pa. The deposited thin films had a nanosized microstructure with grain sizes of 5–20 nm.

Composition Characterization: Energy-dispersive X-ray spectroscopy was performed in a SEM (Jeol 7200 F equipped with an Oxford Inca

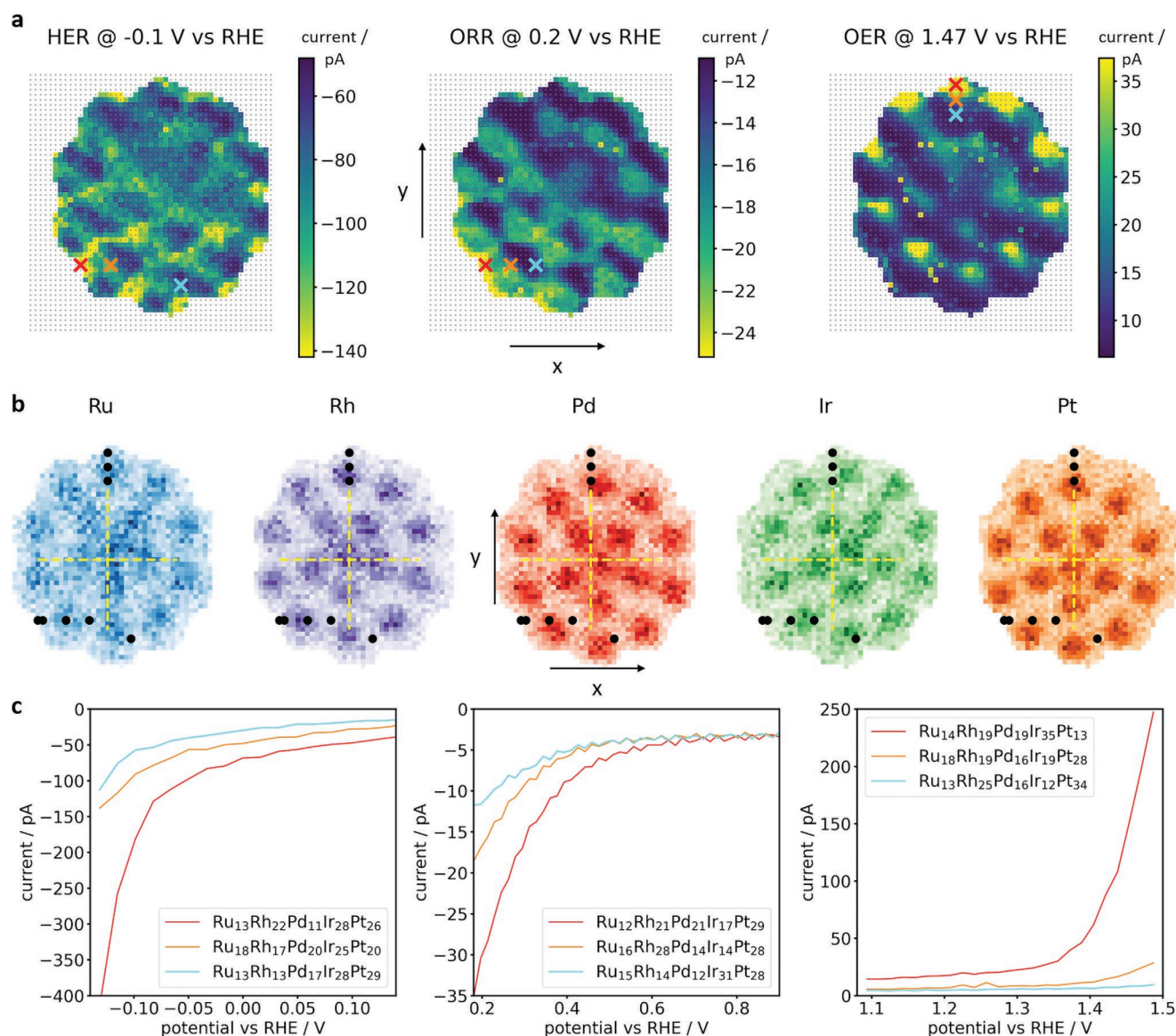


Figure 3. Electrocatalytic activity of a Ru–Rh–Pd–Ir–Pt microlibrary co-deposited through a 16 aperture shadow mask. a) Electrocatalytic activity maps measured on the coordinates of a microlibrary for three different electrocatalytic reactions. The color gradient indicates catalytic currents at –0.1 V versus RHE, 0.2 V versus RHE, and 1.47 V vs RHE for HER, ORR and OER, respectively. The change of the electrocatalytic activity map with a variation of the chosen potential is shown in Movies S1–S3 (Supporting Information). Colored crosses highlight selected SECCM measurement positions. b) Chemical composition maps of a microlibrary, measured by EDX, of the individual elements inside the selected area of a microlibrary. Black circles indicate the positions of the selected SECCM measurements shown in (b) and (c). c) Selected LSV of the measurement areas indicated by crosses in (a) with high (red), medium (orange), and low activity (cyan). An alternative visualization of these results can be found in Figure S7 (Supporting Information).

X-act detector) at a working distance of 10 mm and an acceleration voltage of 20 kV. Auger electron spectroscopy was done on a Phi 710 Scanning Auger Nanoprobe by Physical Electronics. The primary electron energy for the results shown here was 10 kV. Prior to recording the data, the surface was sputter-cleaned using 2 kV Ar⁺ ions to remove contaminations from the surface. The Auger images were 512 × 512 pixel and were recorded in the so-called three-point mode. In this mode, the intensity was measured at the kinetic energy of the respective elemental Auger line. From this, a background signal determined by the measured intensity at two energies at slightly higher and lower kinetic energies, but close to the elemental line, was subtracted. The determined elemental intensities were then corrected with their respective relative sensitivity factors to make the intensities comparable between the different elements.

TEM Characterization: TEM lamellae were prepared using an FEI Helios G4 CX focused ion FIB system operated at 30 kV. Low, 5 kV, ion beam cleaning was applied for 2 min to each side of the TEM lamella in order to remove FIB beam damage. TEM analyses were performed in a Jeol JEM-2100Plus instrument operated at 200 kV equipped with a high-angle annular dark-field (HAADF) detector and an Oxford X-Max EDX spectrometer. All element concentrations were calculated as normalized ratios, based on detector counts. No corrections (for thickness or absorption) were applied.

Electrochemical Measurements: For SECCM probe fabrication, a single barrel nanopipette was pulled from filamented quartz capillaries (ZQF-120-90-10, Science Products) using a CO₂ laser puller (P-2000, Sutter Instruments). The pulling was done with an online program with the following pulling parameters: heat 770, filament 4, velocity

40, delay 130, and pull 100. The size of the nanopipette was measured using scanning electron microscopy (FEI, Quanta 3D ESEM). The tip diameter was ≈ 100 nm. Ag/AgCl quasi reference counter electrodes (QRCE) were fabricated from 0.125 mm Ag wire (Goodfellow, 99.99%) by anodization in a 3 M KCl + 0.1 M HCl solution at +10 V (vs a Pt counter electrode). The Ag/AgCl QRCE were calibrated by measuring the open-circuit potential against a commercial Ag/AgCl [3 M KCl] electrode before and after SECCM measurements. For calibration, the commercial Ag/AgCl [3 M KCl] electrode and the 100 mm HClO₄-filled nanopipette with the Ag/AgCl QRCE inserted were placed inside a one-compartment electrochemical cell filled with 100 mm HClO₄. The open-circuit potential between the two electrodes was measured with a digital potentiometer. The experimental potential values were converted to the RHE reference scale through

$$E_{\text{RHE}} = E + E_{\text{Ag/AgCl [3 M KCl]}} + E_{\text{open-circuit potential correction factor}} + 0.059(\text{pH}) \quad (1)$$

where E is the potential applied to the working electrode (WE), $E_{\text{Ag/AgCl [3 M KCl]}} = 0.210$ V, and pH of 100 mm HClO₄ is 1. The Ag/AgCl QRCE were found to consistently show a potential of 0.4 ± 0.05 V versus RHE.

For SECCM measurement, experiments were performed using a home-built SECCM workstation comprising an x, y, z-piezocube (P-611.3S nanocube, Physik Instrumente) for fine positioning and x, y, z stepper motors (Owis) for coarse positioning of the nanopipette, an optical camera (DMK 21AU04, The Imaging Source), and a cold light source (KL1500 LCD, Schott) for nanopipette and working electrode visualization, a nanopipette holder, and a variable gain transimpedance amplifier (DLPCA-200, FEMTO Messtechnik) for current measurement. The setup was installed in a Faraday cage equipped with thermal isolation panels (Vaku-Isotherm) and placed on a vibration damping table (RS 2000, Newport) with four S-2000 stabilizers (Newport). Data acquisition and instrumental control were carried out using a field-programmable gate array (FPGA) card (PCIe-7852R) controlled by a modified version of the Warwick Electrochemical Scanning Probe Microscopy software provided by the University of Warwick (WEC-SPM) written in LabVIEW (National Instruments).

The SECCM probe (nanopipette filled with 100 mm HClO₄) was approached to the microlibrary, which served as WE mounted on the x, y, z-piezopositioner. A surface current (i_{surf}) threshold of ≈ 2 pA was used to detect when the meniscus contacted the surface of the WE and to stop further translation. Two linear sweep voltammograms were recorded in the confined area defined by the meniscus cell created between the SECCM tip and working electrode surface in the potential range of 1 to -0.2 versus RHE for ORR and HER and 1–1.5 versus RHE for OER. This procedure was repeated at a series of predefined locations in the form of a grid using the standard hopping mode protocol, and upon each landing, independent electrochemical measurements (LSVs) were made thus acquiring a spatially resolved voltammetric (i_{surf} – E) image of the sample (see Figure 3a). Electrochemical and position data extraction and initial plotting, visualization, and analysis were performed using scripts written in Matlab R2020a (Mathworks) software package. All electrochemical/topographical images were presented without any data interpolation.

Supporting Information

Supporting Information is available from the Wiley Online Library or from the author.

Acknowledgements

The authors thank Dr. Bin Xiao for helping with sputter deposition, Dr. Heike Kreher for advising on the photolithographic mask fabrication, and Ellen Suhr for performing complementary composition

measurements and atomic force microscopy. The center for interface dominated high-performance materials (ZGH, Ruhr-Universität Bochum, Bochum, Germany) is acknowledged for access to transmission electron microscopy and scanning electron microscopy. A.L. and L.B. are grateful for funding by the German Research Foundation (Deutsche Forschungsgemeinschaft, DFG) as part of Collaborative Research Center CRC TR 87 (Project No. 138690629). W.S. and O.A.K. are grateful for financial support by the European Research Council (ERC) under the European Union's Horizon 2020 research and innovation programme (CasCat [833408]), and W.S. and E.B.T. are grateful as well for funding from the European Union's Horizon 2020 research and innovation program under the Marie Skłodowska-Curie MSCA-ITN Single-Entity Nanoelectrochemistry Sentinel [812398]. U.H. acknowledges funding by the German Research Foundation (Deutsche Forschungsgemeinschaft, DFG) as part of Collaborative Research Center CRC TR 247 (Project No. 388390466).

Open Access funding enabled and organized by Projekt DEAL.

Conflict of Interest

The authors declare no conflict of interest.

Data Availability Statement

The data that support the findings of this study are available from the corresponding author upon reasonable request.

Keywords

combinatorial electrocatalyst discovery, composition space, electrocatalysis, high-entropy materials, microlibraries

Received: August 21, 2022

Revised: November 19, 2022

Published online:

- [1] E. P. George, D. Raabe, R. O. Ritchie, *Nat. Rev. Mater.* **2019**, *4*, 515.
- [2] F. Huo, Z. Zheng, G. Zheng, L. R. Giam, H. Zhang, C. A. Mirkin, *Science* **2008**, *321*, 1658.
- [3] E. J. Klunder, J. L. Hedrick, K. A. Brown, R. Rao, B. Meckes, J. S. Du, L. M. Moreau, B. Maruyama, C. A. Mirkin, *Proc. Natl. Acad. Sci. USA* **2019**, *116*, 40.
- [4] Y. Yao, Z. Huang, P. Xie, S. D. Lacey, R. J. Jacob, H. Xie, F. Chen, A. Nie, T. Pu, M. Rehwoldt, *Science* **2018**, *359*, 1489.
- [5] J. Feng, D. Chen, P. V. Pikhitsa, Y. Jung, J. Yang, M. Choi, *Matter* **2020**, *3*, 1646.
- [6] Y. Sun, S. Dai, *Sci. Adv.* **2021**, *7*, eabg1600.
- [7] W. A. Saidi, *NPJ Comput. Mater.* **2022**, *8*, 86.
- [8] W. A. Saidi, *J. Phys. Chem. Lett.* **2022**, *13*, 1042.
- [9] W. A. Saidi, W. Shadid, G. Vesper, *J. Phys. Chem. Lett.* **2021**, *12*, 5185.
- [10] J. K. Pedersen, T. A. A. Batchelor, A. Bagger, J. Rossmeisl, *ACS Catal.* **2020**, *10*, 2169.
- [11] W. A. Saidi, T. Nandi, T. Yang, *Electrochem. Sci. Adv.* **2022**, <https://doi.org/10.1002/elsa.202100224>.
- [12] T. A. A. Batchelor, T. Löffler, B. Xiao, O. A. Krysiak, V. Strottkötter, J. K. Pedersen, C. M. Clausen, A. Savan, Y. Li, W. Schuhmann, *Angew. Chem., Int. Ed.* **2021**, *60*, 6932.
- [13] K. Tran, Z. W. Ulissi, *Nat. Catal.* **2018**, *1*, 696.
- [14] A. Ludwig, *NPJ Comput. Mater.* **2019**, *5*, 70.

- [15] X.-D. Xiang, X. Sun, G. Briceno, Y. Lou, K.-A. Wang, H. Chang, W. G. Wallace-Freedman, S.-W. Chen, P. G. Schultz, *Science* **1995**, 268, 1738.
- [16] W. F. Maier, *ACS Comb. Sci.* **2019**, 21, 437.
- [17] S. Curtarolo, G. L. W. Hart, M. B. Nardelli, N. Mingo, S. Sanvito, O. Levy, *Nat. Mater.* **2013**, 12, 191.
- [18] T. D. Hatchard, J. M. Topple, M. D. Fleischauer, J. R. Dahn, *Electrochem. Solid-State Lett.* **2003**, 6, A129.
- [19] J. A. Haber, Y. Cai, S. Jung, C. Xiang, S. Mitrovic, J. Jin, A. T. Bell, J. M. Gregoire, *Energy Environ. Sci.* **2014**, 7, 682.
- [20] L. Banko, O. A. Krysiak, J. K. Pedersen, B. Xiao, A. Savan, T. Löffler, S. Baha, J. Rossmeisl, W. Schuhmann, A. Ludwig, *Adv. Energy Mater.* **2022**, 12, 2103312.
- [21] S. Guerin, B. E. Hayden, *J. Comb. Chem.* **2006**, 8, 66.
- [22] N. Ebejer, A. G. Güell, S. C. S. Lai, K. McKelvey, M. E. Snowden, P. R. Unwin, *Annu. Rev. Anal. Chem.* **2013**, 6, 329.